The Ferrite to Austenite Transformation in Stainless Steels

Given austenite from primary phase ferrite, further decomposition of ferrite to austenite occurs in the solid state by a diffusion controlled mechanism

BY G. L. LEONE AND H. W. KERR

ABSTRACT. The solidification sequence, including the transformation of ferrite to austenite, was studied in stainless steels by optical metallography and microprobe analysis of quenched and continuously cooled samples. Depending on the alloy's composition, secondary austenite can originate in the solid following ferritic solidification or may appear in the liquid through the sequence $L \rightarrow L + \delta \rightarrow L + \delta + \gamma \rightarrow \delta + \gamma$; with $\delta \rightarrow \gamma$ continuing below the solidus line.

When austenite appears in the solid first, it nucleates preferentially at prior grain boundaries of the ferritic matrix, and to a lesser extent at interdendritic locations within the ferrite. When austenite appears in the liquid first, it forms a layer around the primary ferrite dendrites. *In both cases the solid state ferrite to austenite transformation occurs by a diffusion controlled process,* in which Ni diffuses in ferrite towards the advancing austenite, and Cr is rejected by the advancing interface, as demonstrated by the microprobe results. This produces an enrichment of Ni and depletion of Cr in the austenite, compared to the composition of ferrite. In most instances the austenite-ferrite interface becomes non planar, and has a Widmanstatten appearance.

Similarities between the as-cast microstructures and the as-welded microstructures indicate that the solidification models proposed for the as-cast microstructures also can be used to interpret the as-welded microstructure. This conclusion is supported by previously published STEM microanalysis of welds.

Introduction

Many wrought austenitic stainless steels exhibit a duplex austenitic-ferritic structure at room temperature after solidification. The ferrite phase within the austenitic matrix is known to play a beneficial role in the prevention of hot cracking in both as-cast and as-welded structures.

The solidification sequences and solid state phase changes leading to the observed final microstructures have been the subject of extensive investigations, but different interpretations have arisen (Ref. 1-12).

It is now clear, however, that several austenitic stainless steels are either partially or completely ferritic just below the solidus line. The final duplex microstructure at room temperature is strongly dependent on the solidification sequence, the solid state transformation of ferrite to austenite and minor variations in composition (Ref. 14).

The mechanism of the transformation, particularly for certain compositional ranges still remains a controversial issue. Lippold and Savage (Ref. 11,12) have proposed that within a narrow compositional range, for the cooling rate observed in GTA welds, ferrite transforms to austenite by a diffusionless massive transformation. According to this interpretation, the microsegregation observed at room temperature is produced during the liquid to solid transformation, with no further redistribution of elements during cooling of the solid to room temperature. Other authors have instead reported that the ferrite to austenite transformation is diffusion controlled (Ref. 2-9).

In previous investigations, attention has been concentrated on either cast (or slowly solidified) microstructures (Ref. 1-4), or on as-welded microstructures (Ref. 5-12). Since the cooling rates in welds are generally faster than in castings, it has been argued that diffusion may be much more limited in welds, allowing the massive transformation (Ref. 11,12). In the present paper the microstructures and solidification sequences in both cast and welded specimens of certain alloys are examined.

Experimental Procedures

Specimens of both experimental alloys and commercial alloys were studied. The compositions of the alloys referred to in the present paper are listed in Table 1. Casting experiments employed ingots approximately 2.5 mm (1 in.) in diameter and 3 to 4 mm (1.18 to 1.57 in.) high. The alloys were melted under an inert atmosphere, and the cooling curves measured using Pt6Rh-Pt30Rh thermocouples, shielded by alumina tubing. The cooling rate just above the liquidus was approximately 6°C/s (10.8°F/s). Some specimens were quenched into water after solidification had begun in order to examine the development of the microstructure at different temperatures.

Electron microprobe analysis of the cast specimens was carried out using 25 kV accelerating voltage and 100 nA beam current. Chromium and nickel analyses were performed simultaneously. The compositions of individual phases at various locations were determined by point counts, and composition profiles through ferrite-austenite interfaces were examined by line scans. Point counts were

Paper presented at the 62nd AWS Annual Meeting held in Cleveland, Ohio, during April 5-10, 1981.

G. L. LEONE, formerly a graduate student at the University of Waterloo, is with the Deloro Stellite Wear Division, Cabot Corporation, Canada, and H. W. KERR is Professor, Department of Mechanical Engineering, University of Waterloo, Waterloo, Ontario, Canada.

Table 1—Chemical Compositions of Alloys Investigated, Wt-%[a]

Alloys	Cr	Ni	C	N	Mn	Si	S	P	Mo
3	24.3	6.5	0.026	.027	0.76	0.59	0.002	0.012	< 0.1
4	21.0	10.9	0.022	.026	0.71	0.51	0.002	0.011	< 0.1
4½	20.0	11.3	0.03	.017	0.68	0.52	0.003	0.007	< 0.1
304-L	19.3	9.0	0.030	.021	1.7	0.54	< .003	< .045	< 0.1

(a) Remainder Fe.

corrected for fluorescence and absorption using a Magic 4 program developed by Colby (Ref. 13). The corrected values were used to determine redistribution of chromium and nickel during both solidification and the subsequent solid state transformations. Detailed experimental techniques are given elsewhere (Ref. 14).

Autogenous GTA welds were made with a heat input of approximately 1800 J/s at a welding speed of 2.5 mm/s (6 ipm). As in the ingots, thermocouples were placed into the weld pool in order to measure the subsequent thermal history. The cooling rate measured at 1300°C (2372°F) was 100-150°C/s (180-270°F/s).

Results

The transformation of ferrite to austenite in stainless steels can originate either in the solid after ferritic solidification or in the liquid through the solidification sequence $L \rightarrow L + \delta \rightarrow L + \delta + \gamma \rightarrow \delta + \gamma$; with $\delta \rightarrow \gamma$ continuing below the solidus line. The type of freezing mode and subsequent $\delta \rightarrow \gamma$ transformation which results is dictated by the alloy's composition.

Figure 1 defines various compositional regions for a section through the Fe-Cr-Ni ternary phase diagram at a constant iron content of 68 wt-%. Regions I and V, in which solidification is completely ferritic or austenitic respectively, with no subsequent solid state transformations, are not discussed here.

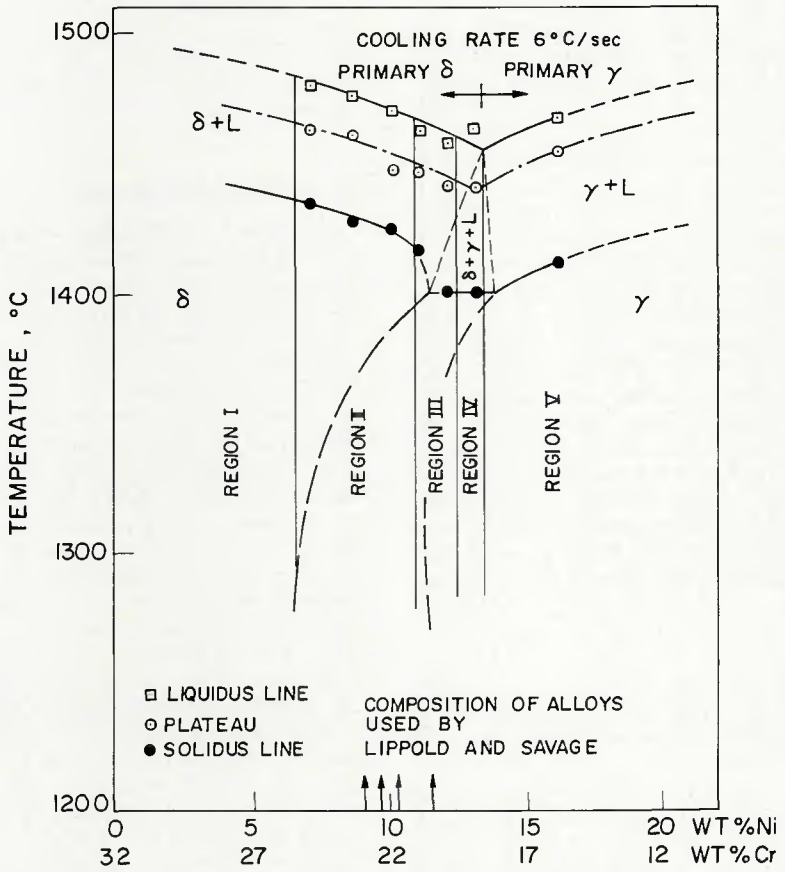

Fig. 1—Pseudobinary section through the Fe-Cr-Ni phase diagram at 68 wt-% Fe, showing the effect of composition on the freezing mode

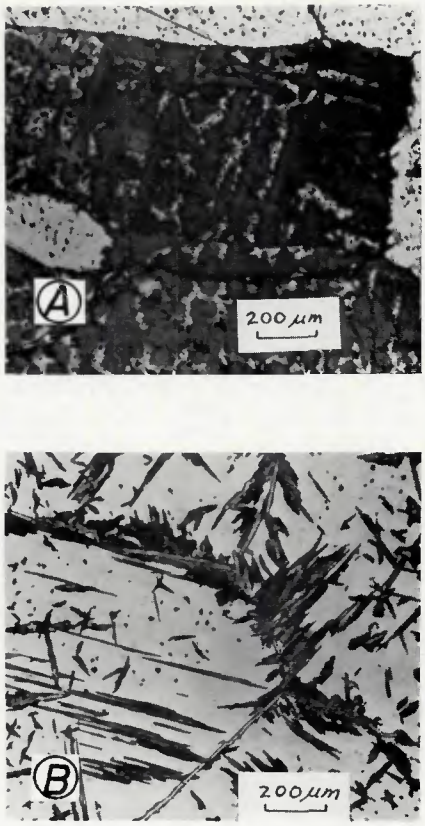

Fig. 2—Microstructures of alloy 3 in cast specimens: A—quenched from 1458°C (2656°F); B—continuously cooled to room temperature

Microstructures of Cast Alloys

Region II

Alloys with compositions within this region solidified completely to ferrite, which on cooling partially transformed to austenite. The freezing mode within this region can be expressed as follows: $L \rightarrow L + \delta \rightarrow \delta$: with $\delta \rightarrow \gamma$ in the solid. Austenite nucleated predominantly at ferrite grain boundaries and to a lesser extent at interdendritic locations within the ferrite.

Figure 2 compares the microstructures of quenched and continuously cooled samples of an alloy with composition close to the left boundary of region II (alloy 3 with Cr/Ni ratio of about 4). These micrographs show that the alloy solidified to δ ferrite (Fig. 2A), which partially transformed to austenite in the solid. Continuously cooled specimens displayed more austenite, without any evidence of solidification microsegregation within the ferrite (Fig. 2B).

The transformation of $\delta \rightarrow \gamma$ at the grain boundaries seemed to have occurred by the formation of an almost continuous layer of austenite along the original ferrite boundaries and then by

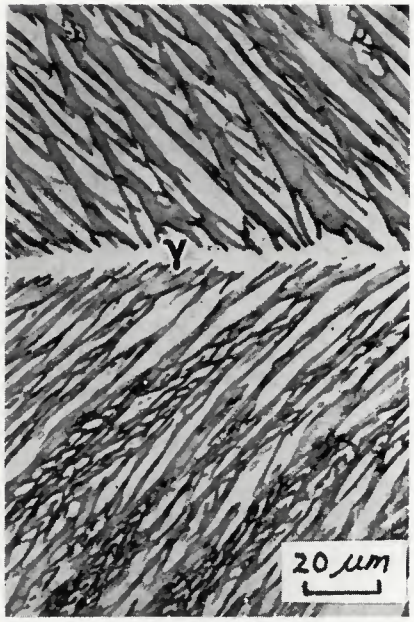

Fig. 3—Microstructure of a continuously cooled specimen of alloy 3 showing austenite Widmanstatten growth morphology

the Widmanstatten growth of this γ layer into δ grains. A grain boundary in a continuously cooled specimen is shown in Fig. 3. Within the grains, on the other hand, the quenched microstructure (Fig. 4) revealed that austenite particles participated in the solid, mostly at the interdendritic regions of ferrite, and grew independently of each other.

The morphological appearance of γ phase in the continuously cooled specimens had all the characteristics of a Widmanstatten structure: precipitation at grain boundaries as well as within the grains, with growth along preferred crystallographic directions giving asymmetrical shapes. As the Cr/Ni ratio decreased, the volume fraction of austenite increased.

Figure 5 compares the microstructures of quenched and continuously cooled samples of an alloy close to the right boundary of region II (alloy 4, with Cr/Ni ratio of about 2). Figure 5A shows dendrites of ferrite that have partially transformed to austenite (white boundary). Electron microprobe results presented later clearly show that the white boundary was austenite, and that it formed in the solid. Figure 5A also shows that ferrite was originally the primary dendritic phase. Note the shape of the γ/δ interface, suggesting the γ growth was initially proceeding with a planar interface, which became unstable at a later stage. The dark wavy δ lines resemble the residual ferrite lines in Fig. 5C.

Figure 5B shows the transformation quenched at an intermediate stage of its development. Coarse austenite has formed at the grain boundary and finer austenite within the grains. The outline of the original δ dendrites within the grains was still discernible due to the remaining microsegregation, allowing easier γ nucleation and growth and hence slightly coarser austenite at previous interdendritic regions. Since the austenite is less continuous in Fig. 5B, the continuous austenite in Fig. 5A must be a quenching effect permitted by the lack of homogenization when quenched from the higher temperature.

With continuous cooling, the transformation of ferrite to austenite occurred throughout and left no large regions of δ ferrite untransformed—Fig. 5C. This resulted in an austenitic matrix with residual δ-ferrite in the form of dark lines, with no resemblance to the original solidification microstructure.

Within region II, decreasing the Cr/Ni ratio (i.e., moving from left to right on Fig. 1) allows austenite to nucleate and grow at higher temperatures, resulting in more and somewhat coarser Widmanstatten austenite (Fig. 5C vs. Fig. 2B). However, the mechanism of the transformation remained the same.

Region III

The solidification sequence of alloys within this region was $L \rightarrow L + \delta \rightarrow L + \delta + \gamma \rightarrow \delta + \gamma$, with $\delta \rightarrow \gamma$ continuing in solid. The austenite formed first in the liquid as a secondary phase enveloping the primary ferrite. On further cooling, it grew into the remaining liquid ($L \rightarrow \gamma$), as well as into ferrite ($\delta \rightarrow \gamma$). The latter reaction continued below the solidus line. The end product of this sequence was a microstructure composed of residual ferrite, essentially along the cores of primary and secondary branches of the former δ dendrites, within an austenitic matrix. The extent to which ferrite transformed to austenite on cooling to room temperature is shown in Fig. 6 for both quenched and continuously cooled specimens of alloy 304-L.

The well-defined dendritic morphology of δ prevailing at high temperature (Fig. 6A) became, on continuous cooling to room temperature, equally spaced lines of a eutectic-like network (Fig. 6B). The spacing between former δ-dendrite branches (Figure 6B) and original δ-branches (Fig. 6A) was similar (50 μ). These micrographs established two important points:

1. Ferrite was the primary phase.
2. Its appearance (eutectic-like network) in the final microstructure was the result of the $\delta \rightarrow \gamma$ reaction during cooling.

A high-magnification micrograph of the remnants of ferrite branches enveloped by a well-defined γ boundary is shown for alloy 4½ in Fig. 7. The micrograph was taken from a region near the solidification front of the quenched sample. The interface between δ and γ (indicated by arrows in Fig. 7) can be taken to represent the point at which γ enveloped δ and grew in both directions; into the remaining liquid ($L \rightarrow \gamma$) and back into the

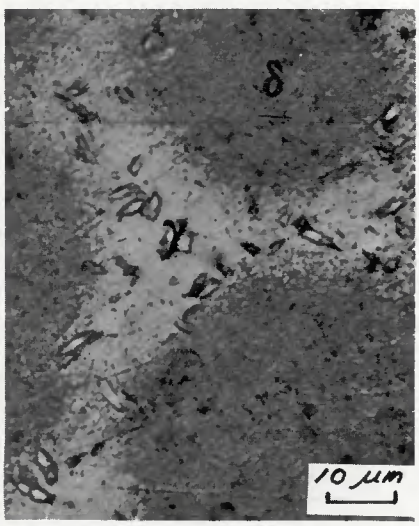

Fig. 4—Microstructure of a specimen of alloy 3 quenched from 1458°C (2656°F), showing austenite nucleation at interdendritic areas

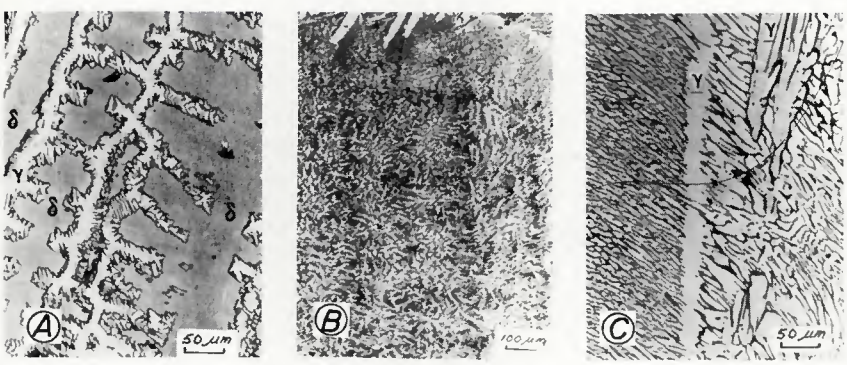

Fig. 5—Microstructures of alloy 4 in cast specimens: A—quenched from 1458°C (2656°F); B—quenched from 1440°C (2624°F); C—continuously cooled ("lathy" ferrite-dark)

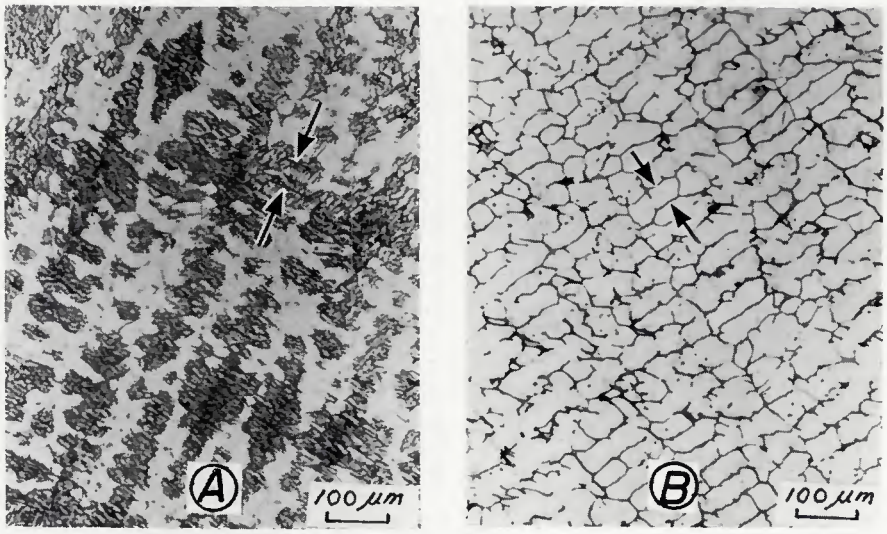

Fig. 6—Microstructures in alloy 304L in cast specimens: A—quenched from 1440°C (2624°F); B—continuously cooled ("vermicular" ferrite-dark)

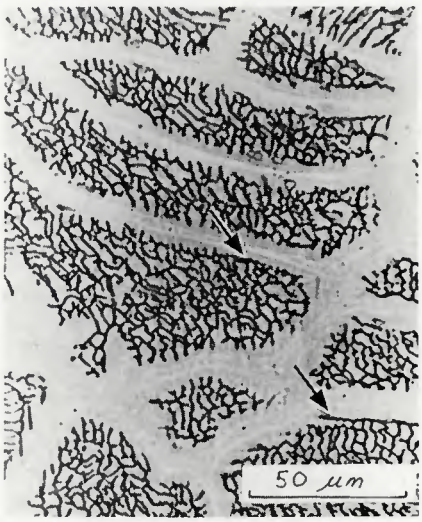

Fig. 7—Microstructure in alloy 4½ quenched from 1458°C (2656°F). The continuous white regions of austenite were the last regions to solidify

ferrite ($\delta \rightarrow \gamma$). The appearance of austenite from the liquid and its growth into δ was supported by electron microprobe results shown later.

Region IV

The freezing mode and resultant room temperature microstructure of alloys within this narrow compositional zone were influenced by both minor variations in composition (including minor elements) and cooling rate. In some cases, austenite formed directly from the liquid, not only as a secondary phase around ferrite, but also as a primary dendritic phase. This mixed mode of solidification is discussed in detail elsewhere (Ref. 15), since the transformation of $\delta \rightarrow \gamma$ in this region played a lesser role in the outcome of the final microstructure.

Solute Distribution in Cast Alloys

Region II

Composition profiles of chromium and nickel recorded from specimens of alloy 3 are reported in Figs. 8-10. The traces show the segregation of Cr and Ni during solidification, as well as their redistribution during the solid state transformation of ferrite to austenite.

The traces in Fig. 8 were taken from one dendrite stem to another in a quenched specimen. The compositional gradient shows an accumulation of Ni and slight depletion of Cr at the interdendritic region (δ inter) indicating that the freezing sequence of alloy 3 was $L \rightarrow L + \delta \rightarrow \delta$, with rejection of Ni and slight absorption of Cr by the solid at the solid-liquid interface.

Figure 9 shows the chromium and nickel variation across a region of the quenched alloy containing a small platelet of γ. The traces reveal that the nickel content drops as the beam approaches the δ/γ interface (shown by dips in the Ni traces) and then rises again when the beam is on the γ particle. The composition profiles of Cr and Ni across a well-defined γ boundary in the continuously cooled ingot show these dips very clearly—Fig. 10. In this case, the variation in Cr content is more apparent than in the previous trace. The austenite layer is richer in nickel and depleted in chromium, compared to ferrite. Moreover, the concentration gradients within ferrite which bring about the required diffusion are also evident.

For alloys closer to region III, the $\delta \rightarrow \gamma$ transformation is more complete in continuously cooled specimens—Fig. 5C. This makes analysis of local compositional gradients very difficult under the electron microprobe, since its resolution is approximately 1 μm. In quenched specimens of such alloys, the transformation may be at least partially arrested—Fig. 5A. A compositional profile from a quenched specimen of alloy 4 showed the same depletion of the Ni and peak in Cr at the δ/γ interface, as well as the segregation between the two phases—Fig. 11. This supports the conclusion that the δ to γ transformation occurred in the solid via a diffusion controlled process for this alloy.

In order to obtain more accurate measurements of the segregation, point counts were made at various locations and corrected for absorption and fluorescence. Table 2 reports data from alloy 4 for two measures of segregation. The first is K_e = (wt-% in ferrite at the dendrite core)/(nominal wt-%). This is a measure of the distribution coefficient K for the selected element,* since the dendrite center should have a composition close to KC_o, where C_o is the average compo-

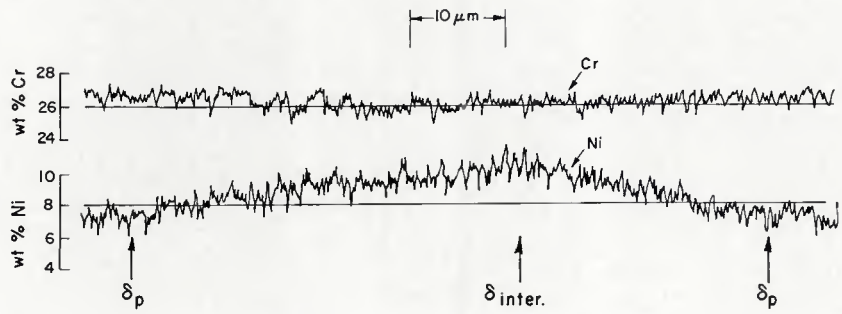

Fig. 8—Cr and Ni microprobe line scans from one dendrite branch to another in a specimen of Alloy 3 quenched from 1458°C (2656°F)

$K = C_s/C_L$ where C_s and C_L are the equilibrium percentages of a given element in the solid and liquid respectively, at a particular temperature.

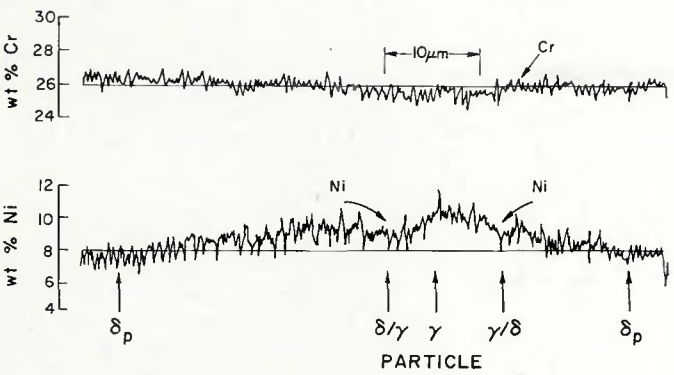

Fig. 9—Electron microprobe concentration profiles of Cr and Ni across a small austenite particle in a specimen of alloy 3 quenched from 1458°C (2656°F)

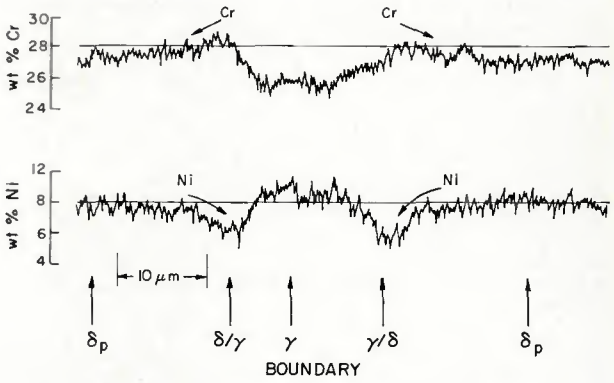

Fig. 10—Concentration profiles of Cr and Ni across a layer of austenite in a continuously cooled specimen of alloy 3

sition (Ref. 11). It can be seen that K_e is less than 1.0 for Ni and greater than 1.0 for Cr, as expected from Fig. 8. However, for both elements, K_e deviates further from 1.0 in the continuously cooled specimen compared to the quenched specimen, showing that redistribution of solute took place within the solid ferrite after solidification.

The other measure of segregation quoted in Table 2 is the partition coefficient P_x, given by: P_x = (wt-% of X in the austenite)/(wt-% of X in the residual ferrite). Since Ni segregates to austenite and Cr to ferrite, $P_{Ni} > 1$ whereas $P_{Cr} < 1$. Comparison of the values of P for quenched versus continuously cooled specimens of alloy 4 (Table 2) also shows that the degree of segregation increased as the ferrite to austenite transformation proceeded. Hence, in the continuously cooled specimen, the segregation between austenite and ferrite is much more marked, consistent with comparison of Figs. 9 and 10.

The interpretation of the traces in Figs. 9-11 is that austenite formed in the solid. If the formation of austenite had taken place from the liquid, an enrichment of chromium in the last region to freeze should be found, as shown below. The transformation of ferrite to austenite is characterized by diffusion of nickel toward the γ/δ interface and the diffusion of chromium away from the γ/δ interface, resulting in an accumulation of Ni and depletion of Cr in the austenite. It is suggested that the concentration profiles of chromium and nickel shown in Figs. 9 and 10 are a characteristic of the solid state transformation of ferrite to austenite and can be used to distinguish between austenite that forms from the liquid and austenite that forms from ferrite in the solid.

The precipitation of austenite at grain boundaries and interdendritic spaces is consistent with the distribution of chromium and nickel within ferrite during solidification. Just below the solidus line, these sites are high in Ni and low in Cr—Fig. 8. This segregation favors the nucleation of austenite, but growth of the austenite requires diffusion as shown by Figs. 9-11.

Region III

Composition profiles from an alloy within this region are shown in Fig. 12. The traces in Fig. 12 are Cr and Ni profiles across residual primary ferrite, γ secondary, and interdendritic γ-boundary for a quenched specimen of alloy 304L (Fig 6A). In going out from the dendrite's center (C), a gradual decrease in Cr and increase in Ni is initially apparent, indicating that chromium segregated to δ ferrite and nickel to liquid, consistent with the solidification of ferrite (Figure 8). Within secondary austenite (Region A), the traces gradually leveled off, and then rose sharply as the beam scanned across the interdendritic region (Region B). Enrichment of both chromium and nickel at the interdendritic boundary results during the solidification of austenite, as shown by microprobe traces for alloys with Region V (Ref. 3,15).

The dip in Ni between γ secondary and interdendritic, i.e., at Point D, may correspond to the initial solid state $\delta \rightarrow \gamma$ transformation, due to γ requiring Ni. In that case, the bottom of the dip would mark the end of ferrite solidification and the beginning of austenite solidification from the liquid.

Within the primary ferrite dendrite, during continuous cooling, after initial δ solidification, segregation of Cr to ferrite and Ni to austenite occurs, giving the valleys and peaks evident at residual ferrite (δp-res) in Fig. 12.

Table 3 summarizes the segregation measured (using point counts) within specimens of alloy 304-L. The K_e values of ferrite for both continuously cooled and quenched from 1440°C (2624°F) specimens show the segregation of Cr to and Ni away from the dendrite centers, consistent with primary ferrite solidification, as shown in alloy 4. Similar to region II, increased segregation is seen for the ferrite at the dendrite core in the continuously cooled specimen compared to the quenched specimen, so that K_e deviates still further from 1.0 for both elements. The partition coefficients, P, are also consistent with the segregation observed between ferrite and austenite in alloy 4, and show reasonable agreement with partition coefficients reported by others (Ref. 2,3).

The segregation shown at the interdendritic region within the austenite shows increases in both Cr and Ni in the

Table 2—Segregation Measured in Alloy 4

History	Coefficients	Cr	Ni
Quenched from 1458°C (2656°F)	K_e[(a)]	1.2	.92
Quenched from 1458°C (2656°F)	$P^{\gamma/\delta}$[(b)]	.88	1.5
Continuously cooled	K_e	1.39	.66
Continuously cooled	$P^{\gamma/\delta}$	.73	1.83

(a) $K_e = \dfrac{\text{wt-\% of X in ferrite at dendrite core}}{\text{average wt-\% of X in alloy}}$

(b) $P^{\gamma/\delta} = \dfrac{\text{wt-\% of X in } \gamma \text{ formed in the solid}}{\text{wt-\% of X in residual primary } \delta}$

Table 3—Segregation Measured in Alloy 304L

History	Coefficients[a]	Cr	Ni	Reference
Quenched	K_e	1.0	0.79	(3)
Quenched from 1440°C	K_e	1.15	0.89	present
Quenched	$p^{\gamma/\delta}$	0.91	1.18	(3)
Quenched from 1440°C	$p^{\gamma/\delta}$	0.93	1.5	present
Continuously cooled	K_e	1.36	0.47	present
Continuously cooled	$p^{\gamma/\delta}$	0.71	2.2	present
Continuously cooled	$p^{\gamma/\delta}$	0.70	2.3	(2)

(a) See Table 2.

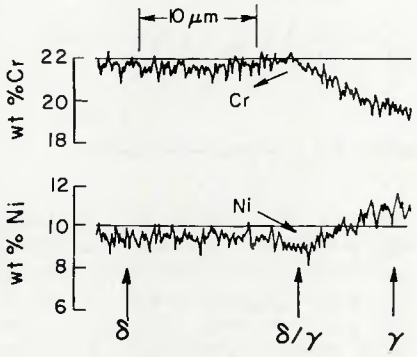

Fig. 11—Microprobe traces of Cr and Ni from ferrite to austenite in a specimen of alloy 4 quenched from 1458°C (2656°F)

last part to freeze—region B in Fig. 12. This is in contrast to ferrite solidification, which shows a slight decrease in Cr content at interdendritic regions—Fig. 8. It is also in contrast to austenite which forms from the solid, which is sharply lower in Cr content compared to ferrite—Figs. 10 and 11. The increase in both Cr and Ni therefore distinguishes austenite which has formed directly from the liquid.

Microstructures of Welds

The room temperature microstructure of welds of alloys within regions II and III exhibited characteristics similar to the cast microstructure.

Region II

Figure 13 shows the weld microstructure of alloy 4 (region II, Cr/Ni ratio of about 2). The microstructure had a Widmanstatten appearance, consisting of $\delta + \gamma$ laths with continuous bands of austenite along the previous ferrite grain boundaries. This type of microstructure, as shown for cast ingots, resulted from the solid state transformation of ferrite to austenite.

Comparison of Fig. 13 with Fig. 5C illustrates the similarity between the weld and cast microstructures. The only significant difference between the two microstructures was the finer spacing between $\delta + \gamma$ laths in the weld structure due to faster cooling rates in welds.

Region III

The microstructure of welds for alloy 304L, shown in Fig. 14, had features similar to the cast structure of alloy 304L and the weld structure of alloy 4½ (Table 1). Ferrite at room temperature was present as partially transformed dendrites, within an austenitic matrix composed of columnar austenitic grains.

The cast results have shown that this type of structure has its origin from the formation of austenite in the liquid as a second phase, and its subsequent growth during cooling to room temperature. The consistency between the cast and weld structures of Alloy 304L suggests that the solidification model proposed from the cast structure can be used to account for the weld structure.

Discussion

The transformation of ferrite to austenite in stainless steels has been shown to originate in two ways: either in the solid after complete solidification to ferrite, or in the liquid after partial solidification to ferrite. In both cases the ferrite to austenite transformation continues below the solidus line. The type of freezing mode and subsequent $\delta \rightarrow \gamma$ transformation which results is dictated by the alloy's composition. For alloys containing approximately 68 wt-% Fe, the regions on the Fe-Cr-Ni pseudo diagram are shown approximately in Fig. 1. Similar compositional regions have been proposed by Lippold and Savage (Ref. 11,12) to explain the weld structures of austenitic stainless steels, but with different interpretations for some regions, as discussed below.

In the alloys studied, the transformation from ferrite to austenite occurred by diffusion of Ni in ferrite towards the advancing γ/δ interface, and of Cr in ferrite away from the advancing γ/δ interface. Therefore, the compositional differences observed at room temperature between ferrite and austenite arose from the partitioning of Cr towards the residual cores of primary ferrite and the partitioning of Ni towards the forming austenite. This is confirmed by the experimental distribution and partition coefficients shown in Tables 2 and 3. These coefficients, for Cr and Ni, for all the alloys in which ferrite decomposed to austenite irrespective of the origin of the austenite, consistently showed that the two elements redistributed during the $\delta \rightarrow \gamma$ reaction. The segregation results are similar to previous investigations of

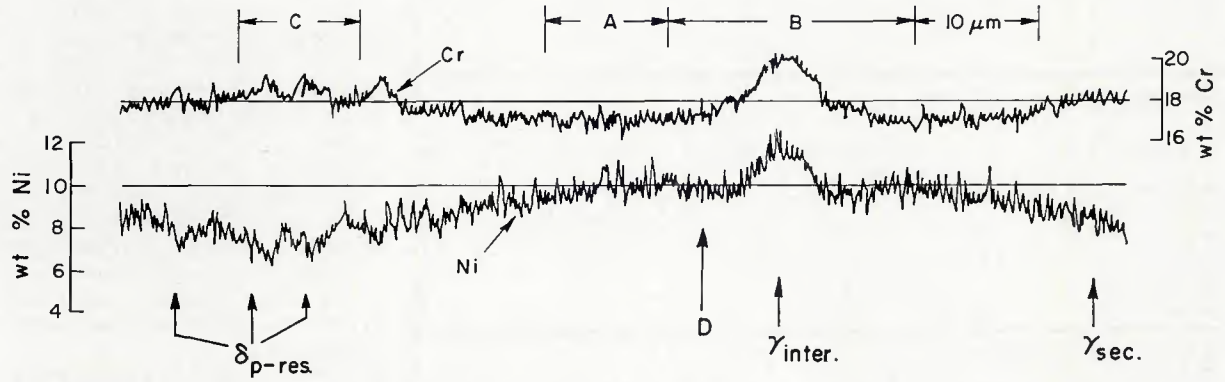

Fig. 12—Line traces of Cr and Ni from a specimen of alloy 304-L quenched from 1440°C (2624°F). Region C is the center of the primary ferrite dendrite, which now contains residual ferrite (δ_p-res). Region B is the interdendritic region, which solidified as austenite

both castings (Ref. 2-4) and welds (Ref. 5-12).

Most authors agree that "lathy" (Widmanstatten) austenite-ferrite structures originate by a diffusion controlled solid state transformation (Ref. 2-9,11,12). However, Lippold and Savage have suggested that some structures termed "acicular" structures which strongly resemble Fig. 13 may originate by a martensitic process (Ref. 12). Moreover, the microstructure typified by continuously cooled alloy 304L (Fig. 6B), often termed "vermicular" (Ref. 6-8,11,12) has been ascribed to a massive transformation in several recent publications (Ref. 10,12). The present results instead lead to the conclusion that vermicular ferrite results when austenite originates in the liquid, and then grows into the solid ferrite by a diffusion controlled transformation. Several aspects of the arguments used by Savage and co-workers (Ref. 10,12) must be examined in assessing their conclusion that vermicular ferrite remains after a diffusionless massive transformation.

There is no doubt that cooling rates are generally faster in welds than in castings, allowing less time for diffusion. It should be noted, however, that the cooling rates affect both liquid and solid state diffusion. Since dendrite spacings are determined by liquid diffusion, they are also reduced by the faster cooling rates in welds. Hence the distances over which diffusion must take place to bring about a solid state phase transformation are smaller in welds.

The present investigation employed microprobe analysis, whereas Lippold and Savage employed STEM analysis which is capable of finer resolution. The finer segregation in the welds cannot be analyzed on the microprobe. However, STEM analysis of welds by both David, *et al.* (Ref. 9) and Lyman (Ref. 10) showed the same sort of concentration profiles reported here within the ferrite at the austenite-ferrite interface (i.e., a gradient of Ni towards γ and a gradient of Cr away from γ) as in Figs. 9-11. This is consistent with the conclusion that the austenite to ferrite transformation remains diffusion controlled in welds.

In order to fit their results to the solidification microsegregation model which they employed, Lippold and Savage (Ref. 11) assumed values of the distribution coefficients of 0.4 for Ni and 1.3 for Cr. Comparison with Table 3 shows that these values are close to the values of K_e for residual ferrite measured in continuously cooled 304-L specimens. However, specimens quenched from higher temperatures showed distribution coefficients for ferrite solidification closer to 1.0; Tables 2 and 3 show $K_e \sim 0.9$ for Ni and $K_e \sim 1.15$-1.2 for Cr, consistent with values reported by other workers for quenched specimens (Ref. 3,4). Hence the distribution coefficients assumed by Lippold and Savage, particularly that for Ni, are affected by solid state diffusion.

In their analysis of the microsegregation, Lippold and Savage have assumed that solidification takes place with no diffusion in the solid. In order to justify this assumption, they have employed the microsegregation measured by Lyman (Ref. 10) which shows a very sharp peak of Cr and valley in Ni at ferrite particles, over a distance less than 0.5 μm wide. In analyzing the diffusion which may take

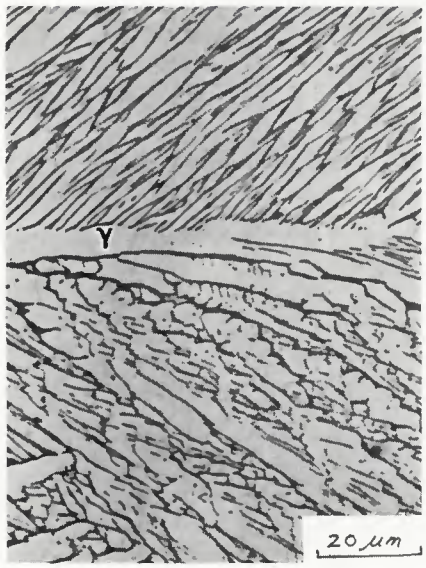

Fig. 13—Microstructure of a GTA weld in alloy 4. Compare to Fig. 5C

place they have quoted a cooling rate of 1000°C/s (1800°F/s).

Our experiments measured a cooling rate at 1300°C (2372°F) of up to 150°C/s (270°F/s) in GTA welds. Conductive heat transfer analysis (Ref. 16) shows that the cooling rate for a partial penetration weld is proportional to $(T - T_o)^2$ where T is the temperature in question and T_o is the ambient temperature in the specimen where heating has not occurred. Using this correction factor, the cooling rate at 1450°C (2642°F) (just below the liquidus) is calculated to be approximately 200°C/s (360°F/s) in the present GTA welds. Hence compared to the assumed cooling rate of 1000°C/s (1800°F/s), the time available for diffusion would be increased by approximately a factor of 5. Following the usual rule of thumb (Ref. 11) that the diffusion distance equals 2 $(Dt)^{1/2}$, where D is the diffusion coefficient and t is the time available for diffusion, the slower cooling rate would allow the diffusion distance to increase by approximately a factor of 2.

In addition, the total diffusion distance is actually determined by the sum of the diffusion which may take place as the temperature drops, i.e., $\Sigma_i D_i t_i$ where D_i is the diffusion coefficient and t_i is the time spent in the i^{th} subintervals (Ref. 17). This results in a diffusion distance of $2(\Sigma_i D_i t_i)^{1/2}$.

Lippold and Savage employed diffusion coefficients for austenite in their analysis (Ref. 11). The diffusion coefficients in ferrite are approximately 50 to 100 times greater than those in austenite at any given temperature (Ref. 18-20). Calculations of the diffusion coefficients of Ni in ferrite measured by Moharil, *et al.* at very high temperatures (Ref. 20), using the cooling rates calculated from the present experiments in GTA welds, give the results shown in Table 4. From these calculations the estimated diffusion distance $[2(\Sigma_i D_i t_i)^{1/2}]$ for Ni in ferrite is approximately 4.4 μm. This is much larger than the value of 0.08 μm quoted by Lippold and Savage. It is also considerably larger than the width of the segregation peaks within GTA welds observed by Lyman (Ref. 10).

Diffusion data which has been measured at lower temperatures is available for both Cr and Ni in ferrite (Ref. 18,19). If the data for Cr (Ref. 19) is extrapolated to 1420°C (2588°F), even if the constant cooling rate of 1000°C/s (1800°F/) is assumed following Lippold and Savage (Ref. 11), the diffusion distance is calculated to be 0.90 μm (Table 5), i.e., approximately 10 times greater than that calculated by Lippold and Savage, and again greater than the width of the peaks observed by Lyman. Hence even for a cooling rate which is approximately 5 times faster than was measured in the present experiments, the calculated diffusion distances are great enough to considerably broaden any initial peaks in microsegregation due to solidification. It is concluded that the microsegregation measured by Lyman, in GTA welds of austenitic stainless steels containing ferrite, arose during solid state diffusion, rather than being that produced directly by solidification.

The diffusion distances calculated above are smaller than the observed spacing of dendrite arms in GTA welds in stainless steels. In the present experiments, the dendrite spacings in the welds were approximately 10 μm, consistent with the spacing measured between ferrite particles by Lyman (Ref. 10). If the ferrite to austenite transformation were to occur with a planar interface, then the width of the transformed austenite would be limited to the approximate diffusion distances, i.e., 0.9-4.5 μm, as discussed above. In order to solve this diffusion problem, the ferrite-austenite interface generally breaks down to a nonplanar morphology. This breakdown is analogous to the formation of den-

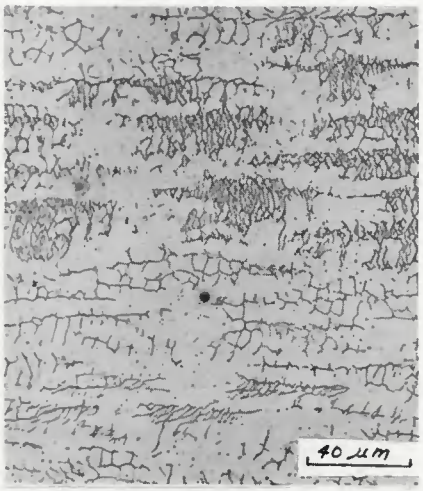

Fig. 14—Microstructure of a GTA weld in alloy 304-L

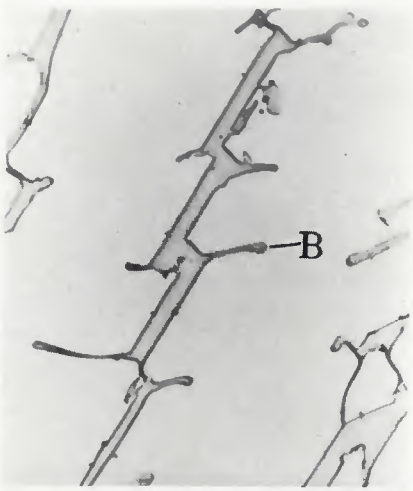

Fig. 15—Residual ferrite at dendrite cores in a specimen of alloy 304-L quenched from an intermediate temperature. The nonplanar γ-δ interface is apparent, and spherodizing of ferrite is seen at B

drites in solidification (Ref. 21). As the nonplanar austenite interface advances, it leaves Cr-rich and Ni-depleted ferrite in between, analogous to solidification microsegregation.

In cast structures the nonplanar nature of the interface was very clear—Fig. 15. Because of the high surface to volume ratio of the residual ferrite, it attempts to spherodize. Figure 15 shows a region (B) which was in the process of spherodizing prior to being quenched. When sufficient time is available, the small ferritic regions shrink back towards the cores of the primary and secondary ferrite branches, which remain untransformed. The nonplanar nature of the original ferrite-austenite interface, followed by partial spherodization, produce the rounded wavy "vermicular" pattern of ferrite found in region III.

The spacing between ferrite in region II, i.e., "lathy" (Ref. 6-8) ferrite, is generally finer than the spacing in vermicular ferrite. The growth of austenite in region II occurs at lower temperatures than in region III (Fig. 1) so that the diffusion coefficients which determine the spacing are smaller. Suutala, *et al.* have also indicated that no orientation relationship exists between the two phases for vermicular ferrite, whereas distinct orientation relationships do occur for lathy ferrite (Ref. 8). Distinct orientation relationships may limit the mobility of the δ-γ interface, forcing the transformation to occur at lower temperatures with finer spacings.

Adjacent regions sometimes exhibit different ferrite spacings—Fig. 14. Similar mixtures of spacings have been observed by Suutala, *et al.* (Ref. 6,8). This may be a result of being very close to the border between regions II and III. If the liquid layer around the ferrite dendrites is not uniform in thickness, then some regions may actually solidify entirely to ferrite while others finish with austenite solidification. Alternatively different habit planes and growth directions between δ and γ may affect interface mobility and hence ferrite spacing.

Conclusion

Both cast and welded microstructures have been examined in austenitic stainless steel alloys in which the primary phase was ferrite. Depending on the

Table 4—Calculated Diffusion of Ni in Ferrite

Temperature Interval, °C	Cooling Rate, °C/s[a]	Time in temperature intervals, t_i(s)	Average D_i, cm²/s[b]	$D_i\ t_i$ (cm²)
1440-1400	178	0.22	7.8×10^{-8}	1.71×10^{-8}
1400-1300	161	0.62	3.49×10^{-8}	2.16×10^{-8}
1300-1200	138	0.72	9.74×10^{-9}	0.70×10^{-8}
1200-1100	117	0.85	2.27×10^{-9}	0.19×10^{-8}
1100-1000	97	1.03	4.24×10^{-10}	0.04×10^{-8}
			$\Sigma_i D\ t_i = 4.8 \times 10^{-8}$ cm²	
			$2\ (\Sigma_i D_i\ t_i)^{1/2} = 4.4\ \mu$m	

(a) Cooling rate ≃ 150°C/s at 1300°C; corrected at other temperatures, see text.
(b) $D_{Ni} = 9.7 \exp(-62{,}700/RT)$ (Ref. 20).

Table 5—Calculated Diffusion of Cr in Ferrite at 1000°C/s Cooling Rate.

Temperature, °C	Cooling Rate, °C/s[a]	Time in temperature interval, t_i(s)	Average D_i, cm²/s[b]	$D_i\ t_i$(cm²)
1440-1400	1000	0.04	1.70×10^{-8}	6.83×10^{-10}
1400-1300	1000	0.1	8.92×10^{-9}	8.92×10^{-10}
1300-1200	1000	0.1	3.17×10^{-9}	3.17×10^{-10}
1200-1100	1000	0.1	9.79×10^{-10}	0.97×10^{-10}
1100-1000	1000	0.1	2.52×10^{-10}	0.25×10^{-10}
			$\Sigma_i D\ t_i = 2.01 \times 10^{-9}$ cm²	
			$2(\Sigma_i D_i\ t_i)^{1/2} = 0.9\ \mu$m	

(a) As assumed by Lippold and Savage (Ref. 11).
(b) $D_{cr} = 0.06 \exp(-50700/RT)$ (Ref. 19).

steel's composition, austenite has been shown to originate in two ways; either from the liquid as the secondary phase, or in the solid.

In both cases further decomposition of ferrite to austenite occurred in the solid state by a diffusion controlled mechanism. During this solid state process the growth of austenite was accompanied by the rejection of Cr and the acceptance of Ni, resulting in an enrichment of Cr and depletion of Ni in the residual ferrite.

The solidification of primary ferrite was shown in specimens quenched from just below the liquidus, to take place with distribution coefficients for Ni and Cr of approximately 0.9 and 1.15-1.2 respectively, whereas the solidification of austenite was accompanied by a build-up of both Cr and Ni in the last region to freeze. This simultaneous increase in both Cr and Ni distinguishes austenite which has formed from the liquid from that formed from the solid, in which the Cr content is low compared to residual ferrite.

During the solid state ferrite to austenite, the build up of Cr and depletion of Ni in the residual ferrite gives apparent distribution coefficients of approximately 1.4 for Cr and 0.5 to 0.7 for Ni. However, these values do not represent the distribution coefficients for solidification of ferrite.

The solidification sequences and subsequent solid state transformations may be represented on a pseudo-binary section of the ternary Fe-Cr-Ni phase diagram as five different regions. In region II the austenite originates in the solid state, initiating at ferrite grain boundaries and growing into the grain centers by Widmanstatten growth, producing "lathy" residual ferrite. In region III the austenite originates in the liquid as a layer around the primary ferrite dendrites. Growth of austenite into ferrite eventually produces a nonplanar interface. Partial spherodization of the residual ferrite produces a wavy "vermicular" form centered at the cores of the primary dendrites of ferrite.

No evidence was found for massive or martensitic transformations in the alloys studied. Reanalysis of the evidence for the massive transformation postulated earlier suggests instead that the observed ferrite was residual ferrite following a diffusion controlled solid state transformation.

Acknowledgments

The financial support for this work from the Natural Sciences and Engineering Research Council Canada is gratefully acknowledged. Mr. J. Kamler provided useful assistance with the electron microprobe work. Chemical analysis was carried out by Ontario Hydro.

References

1. Castro, R. 1961. Sur la structure secondaire des aciers inoxydables austenitiques. *Mem. Sci. Rev. Met.* 58 (11): 881-884.

2. Blanc, G., and Tricot, R. 1971. Solidification, segregation et homogeneisation des aciers inoxydables austenitiques contenant de la ferrite delta. *Mem. Sci. Rev. Met.* 58 (11): 735-753.

3. Fredriksson, H. 1972. The solidification sequence in an 18-8 stainless steel, investigated by directional solidification. *Met. Trans.* 3 (11): 2989-2997.

4. Hammar, O., and Svensson, U. 1979. Influence of steel composition on segregation and microstructure during solidification of austenitic stainless steels. *Solidification and Casting of Metals.* 401-410. London: The Metals Society.

5. Arata, Y., Matsuda, F., and Katayama. 1976. Solidification crack susceptibility in weld metals of fully austenitic stainless steels. *Trans. JWRI* 5 (2): 35-51.

6. Suutala, N., Takalo, T., and Moisio, T. 1979. The relationship between solidification and microstructure in austenitic and austenitic-ferritic stainless steel welds. *Met. Trans.* 10A (4): 512-514.

7. Suutala, N., Takalo, T., and Moisio, T. 1979. Single-phase ferritic solidification mode in austenitic-ferritic stainless steel welds. *Met. Trans.* 10A (8): 1183-1190.

8. Suutala, N., Takalo, T., and Moisio, T. 1980. Ferritic-austenitic solidification mode in austenitic stainless steel welds. *Met. Trans.* 11A (5): 717-725.

9. David, S. A., Goodwin, G. M., and Braski, D. N. 1979. Solidification behaviour of austenitic stainless steel filler metals. *Welding Journal* 58 (11): 1979, Research Suppl. 330-S to 336-S.

10. Lyman, C. E., Analytical Electron Microscopy of Stainless Steel Weld Metal, *Welding Journal,* 58 (7): 189-s to 194-s.

11. Lippold, J. C., and Savage, W. F. 1979. Solidification of austenitic stainless steel weldments part 1—a proposed mechanism. *Welding Journal* 58 (12): 362-s to 374-s.

12. Lippold, J. C., and Savage, W. F. 1980. Solidification of austenitic stainless steel weldments: part 2—the effect of alloy composition on ferrite morphology. *Welding Journal* 59 (2): 48-s to 58-s.

13. Colby, J. W., MAGIC—*a computer program for quantitative electron microprobe analyses.* Allentown, Pa.: *Bell Telephone Laboratories.*

14. Leone, G. L. 1980. *Solidification models and grain structure of normally austenitic stainless steels.* Ph.D thesis. Waterloo, Ontario: University of Waterloo.

15. Leone, G. L., and Kerr, H. W., to be published.

16. Adams, C. M. Jr. 1958. Cooling rates and peak temperatures in fusion welding. *Welding Journal* 37 (5): 210-s to 215-s.

17. Geiger, G. H., and Poirier, D. R. 1973. *Transport phenomena in metallurgy,* p. 500. Reading, Mass.: Addison-Wesley.

18. Hirano, K., Cohen, M., and Averbach, B. L. 1961. Diffusion of nickel into iron. *Acta Met.* 9 (5): 440-445.

19. Smith, A. F., and Hales, R. 1976. The diffusion of chromium in a duplex alloy steel. *Metal Science* 10 (12): 418-423.

20. Moharil, D. B., Jin, I., and Purdy, G. R. 1974. The effect of δ-ferrite formation on the post-solidification homogenization of alloy steels. *Met. Trans.* 5 (1): 59-63.

21. Shewmon, P. G. 1969. *Transformations in Metals,* p. 219. New York: McGraw-Hill.

WRC Bulletin 265
February 1981

Interpretive Report on Small-Scale Test Correlations with K_{ic} Data

by R. Roberts and C. Newton

Correlations of Charpy test results for the upper shelf region and three types of transition region correlations are evaluated. The efforts of plate position and scatter of the experimental results are also noted. The materials reviewed are steels with yield strengths between 250 and 760 MPa (36 and 100 ksi).

Publication of this report was sponsored by the Subcommittee on Effective Utilization of Yield Strength of the Pressure Vessel Research Committee of the Welding Research Council.

The price of WRC Bulletin 265 is $10.00 per copy, plus $3.00 for postage and handling. Orders should be sent with payment to the Welding Research Council, 345 E. 47th St., Room 801, New york, NY 10017.

WRC Bulletin 268
June 1981

Review of Worldwide Weld Discontinuity Acceptance Standards

by C. D. Lundin

In this report the approach to the significance of weld discontinuities taken by foreign code writing bodies is surveyed and contrasted as appropriate to the U. S. efforts.

Extracts of the British and Japanese approaches are presented. The literature available from Japan is given special citing. A comparison between ASME and selected French and German codes is also documented with regard to various inspection methods.

Publication of this report was sponsored by the Subcommittee on Significance of Weld Discontinuities of the Pressure Vessel Research Committee of the Welding Research Council.

The price of WRC Bulletin 268 is $10.75 per copy plus $3.00 for postage and handling. Orders should be sent with payment to the Welding Research Council, 345 E. 47th St., Room 801, New York, NY 10017.

WRC Bulletin 269
August 1981

Interpretive Report on Dynamic Analysis of Pressure Components—Second Edition

This report is the first update of WRC Bulletin 246, February 1979. It summarizes the state-of-the-art in the four most important areas of dynamic analysis: 1) Dynamic Modeling; 2) Pipe Rupture Phenomena and Missile Impact; 3) Fluid Pressure Transients; and 4) Seismic Analysis and Related Effects.

This Second Edition was prepared by the Subcornmittee on Dynamic Analysis of Pressure Components of the Pressure Vessel Research Committee. It will be used as a guide for all future research of the Subcommittee to help avoid duplication of effort.

The price of WRC Bulletin 269 is $10.75 per copy plus $3.00 for postage and handling. Orders should be sent with payment to the Welding Research Council, 345 E. 47th St., New York, NY 10017.